Available online at www.sciencedirect.com
SCIENCE DIRECT®
Journal of Solid State Chemistry 179 (2006) 1469–1477
JOURNAL OF SOLID STATE CHEMISTRY
www.elsevier.com/locate/jssc

The defect chemistry of $Ce(Pr, Zr)O_{2-\delta}$

D.P. Fagg*, J.R. Frade, V.V. Kharton, I.P. Marozau

Department of Ceramics and Glass Engineering, CICECO, University of Aveiro, 3810-193 Aveiro, Portugal

Received 18 October 2005; received in revised form 10 January 2006; accepted 28 January 2006
Available online 28 February 2006

Abstract

The influence of composition upon resultant mixed conductivity is analysed for the fluorite-type compositions $Zr_{0.1}Ce_{0.7}Pr_{0.2}O_{2-\delta}$, and $Ce_{0.8}Pr_{0.2}O_{2-\delta}$. Measurements of oxygen concentration cell e.m.f. combined with impedance spectroscopy at elevated temperatures reveal the materials to be predominantly ionic conductors in oxidising conditions and to show a decrease in both ionic and electronic conductivities with decreasing pO_2. Ion transference numbers measured under these conditions show a positive temperature dependence, with typical values $t_0 = 0.8$ and 0.9, respectively, for the two compositions at 950 °C. The combination of this information with results of coulombic titration, facilitates analysis of the pO_2 dependence of total conductivity measured by a steady-state electrochemical technique between air and reducing conditions. In more oxidising conditions, depletion of total conductivity with decreasing pO_2 results predominantly from a decreasing ionic conductivity. This is one of first examples in the literature where a fluorite-type material is shown indisputably to exhibit such behaviour. These materials show significant levels of mixed conductivity in both reducing and oxidising conditions. In more reducing conditions, an increase in total conductivity is related to increased n-type conductivity upon the reduction of cerium.

Keywords: Praseodymium-cerium oxide; Transference number; Mixed conduction; Defect chemistry; Ionic conductivity

1. Introduction

Interest has been shown for the use of ceria-based oxides as possible oxygen separation membranes, components for solid oxide fuel cells (SOFC), amperometric oxygen sensors and oxygen storage materials. Of these studies, the solid solution system $Ce_{1-x}Pr_xO_{2-\delta}$ has generated attention due to its ability to accommodate extensive deviations from stoichiometry with high rates of oxygen exchange and diffusion, whilst offering good stability in repeated redox cycles, all features of great importance for use as gas sensors, catalyst supports and/or oxygen storage materials in automotive catalysis [1–7]. These materials may also be promising for oxygen separation membranes, with oxygen permeabilities rivalling that of mixed conductors based on the best conductive bismuth oxide solid electrolytes [8]. To maximise oxygen flux through an oxygen separation membrane, mixed conductors that offer equally high electronic and ionic conductivities are required. Shuk and Greenblatt [8] demonstrated that at Pr concentrations greater than 25 at% Pr the electronic conductivity of the system $Ce_{1-x}Pr_xO_{2-\delta}$ in air starts to exceed that of the ionic conductivity, yielding theoretical values of oxygen permeability for this material, $J(O_2) = 1.9 \times 10^{-10}$ mol/scm at 700 °C.

Unfortunately the binary system, $Ce_{1-x}Pr_xO_{2-\delta}$, is blighted by a high and non-linear thermal expansion, for example, the average thermal expansion coefficient (TEC) observed by dilatometry for the material $Ce_{0.8}Pr_{0.2}O_{2-\delta}$ is reported to vary between 10 and $30 \times 10^{-6}\,K^{-1}$ across different temperature ranges between 0 and 1000 °C [9,10]. Such a fluctuation of TEC clearly limits possible practical uses. However, recent work by our group [11] has shown that the extremely high TEC observed at intermediate temperatures in these materials has its root in the loss of oxygen upon heating and can be substantially decreased by the substitution 10 at% Zr for cerium. For example, upon substitution of 10 at% Zr for cerium to form the composition $Zr_{0.1}Ce_{0.7}$ $Pr_{0.2}O_{2-\delta}$, average TECs varying

*Corresponding author. Fax: +351 234 425300.
E-mail address: duncan@cv.ua.pt (D.P. Fagg).

0022-4596/$ - see front matter © 2006 Elsevier Inc. All rights reserved.
doi:10.1016/j.jssc.2006.01.052

between 13 and $18 \times 10^{-6} K^{-1}$ across the temperature range 30–1000 °C can be offered. Zirconium substitution was shown to increase average grain size, to decrease lattice parameter and to also have the negative effect of decreasing total conductivity in air. To understand this phenomenon further, we assess the influence of zirconium substitution on resultant average Pr oxidation state and study its dependence on oxygen partial pressure by use of the coulombic titration technique. Uniting these results with ion transference numbers obtained by oxygen concentration cell e.m.f. under various oxygen chemical potential gradients, will allow analysis of the pO_2 dependence of total conductivity measured for compositions $Zr_{0.1}Ce_{0.7}Pr_{0.2}O_{2-\delta}$, and $Ce_{0.8}Pr_{0.2}O_{2-\delta}$ by a steady-state electrochemical technique.

2. Experimental

2.1. Sample preparation

Stoichiometric amounts of high-purity Pr_6O_{11}, $ZrO(NO_3)_2 \cdot H_2O$, and $Ce(NO_3)_3 \cdot 6H_2O$ were dissolved in a hot aqueous solution of nitric acid. After drying, the nitrate mixture was decomposed at 700 °C. The resultant powder was ball-milled in a nylon mill with zirconia balls. The milled powder was dry pressed into pellets (diameter of 20 mm, pressure of 30 MPa) followed by isostatic pressing at 200 MPa. These pellets were then sintered at 1600 °C for 10 h followed by cooling at 2 °C/min. The density of materials synthesised from their component metal nitrates was greater than 90% that of the theoretical density in every case. All samples were gas tight. Overall phase composition was determined by X-ray diffraction (XRD) using a Rigaku Geigerflex diffractometer (Cu$K\alpha$ radiation), (5–80°, step 0.02, 0.4 s/step); unit cell parameters were determined using Materials Data Inc. Jade6 software, pseudo voight profile fit and an external silicon standard for zero point correction, Table 1. All samples were single-phase cubic defect fluorite.

2.2. Electrical characterisation

Total conductivity was performed on dense bars, approximately 2 mm × 4 mm × 12 mm using the 4-point d.c. method as described elsewhere [12]. The measurements were carried out in a controlled atmosphere device consisting of a yttria-stabilised zirconia (YSZ) cell with an electrochemical oxygen pump and a sensor [12]. At the start of the experiment, the cell was filled with a gas mixture containing 50% of O_2 and 50% of CO_2 and then sealed. The conductivity was measured using a voltmeter Solartron 7081 in the temperature range 750–950 °C at oxygen partial pressures from 10^{-19} to 0.5 atm. Precise variation or maintenance of the partial oxygen pressure in the chamber was provided by the operation of the oxygen pump and sensor, controlled by a computer using specially developed software. The measurements were carried out in the mode of decreasing oxygen partial pressure in isothermal runs. When maintaining a constant oxygen pressure in the well-known instability range [13] corresponding to the electrochemical sensor e.m.f. from approximately 200 to 650–700 mV, the operation regime of the oxygen pump utilised provided the sensor e.m.f. constant with an accuracy of ±2 mV. Experimental data points were collected upon achievement of equilibrium between the sample and ambient atmosphere; the criterion of the equilibrium achieved was a conductivity relaxation rate less than 0.1% per minute, under a fixed oxygen pressure inside the chamber. The conductivity relaxation time after a change in the oxygen pressure over a sample varied up to several hours, depending on temperature, oxygen partial pressure and sample composition. As a rule, the conductivity relaxation time in the instability range was no less than 1 h; the total time necessary for one isothermal measurement cycle was 20–70 h. The above-described criteria are believed to ensure that the obtained conductivity data correspond to equilibrium oxygen content in the samples. Upon achievement of the desirable low oxygen-pressure limit, the measurements were halted and then the oxygen pressure was increased to the starting upper limit, where the measurements were repeated in order to confirm reversibility of the experiment; thereupon temperature was changed thus enabling next measuring cycle. Simultaneous measurements of thermoelectric power were obtained as described elsewhere [12].

Trace electron–hole conductivity was separated from total electrical conductivity using the modified e.m.f. method first proposed by Gorelov [14]. This modification of the classical e.m.f. technique, based on determination of the open-circuit voltage of oxygen concentration cells, increases measurement sensitivity and eliminates possible errors in the determination of ion transference numbers

Table 1
Lattice parameter and relative density of $Ce_{1-x}Pr_xO_{2-\delta}$ and $Zr_{0.1}Ce_{0.9-x}Pr_xO_{2-\delta}$ ceramics as prepared in air, together with activation energies for the partial ionic conductivities of $Ce_{0.8}Pr_{0.2}O_{2-\delta}$ and $Zr_{0.1}Ce_{0.6}Pr_{0.2}O_{2-\delta}$ ceramics in the oxygen potential gradients 101/21 kPa and 21 kPa/20 Pa

Composition	Relative density (%)	Lattice parameter (nm) (±0.0004)	E_a ionic (kJ mol^{-1})	
			101/21 kPa	21 kPa/20 Pa
$Ce_{0.8}Pr_{0.2}O_{2-\delta}$	92.7	0.5437	60.9	62.2
$Zr_{0.1}Ce_{0.7}Pr_{0.2}O_{2-\delta}$	96.5	0.5421	61.2	65.4

arising due to electrode polarisation, errors that are shown to be nonnegligible for electrolyte-type materials which possess relatively minor electronic conductivity [15,16]. The experimental set-up, measurement procedure and also comparison of this technique with the traditional approach are well documented in the literature [15,16].

2.3. Characterisation of oxygen nonstoichiometry

The oxygen content variations with respect to a reference point were measured as a function of oxygen partial pressure and temperature by means of the coulometric titration technique in the double electrochemical cell in potentiostatic mode, as described elsewhere [17]. The potentiostatic mode has the benefit that the unavoidable leakage current I_{leak} is given by the value to which the current decays after a potentiostatic step. The change in sample oxygen nonstoichiometry, $\Delta\delta$, is given by the integration of the current over time [18].

3. Results and discussion

3.1. Oxygen nonstoichiometry

The coulometric titration results for compositions $Zr_{0.1}Ce_{0.7}Pr_{0.2}O_{2-\delta}$, and $Ce_{0.8}Pr_{0.2}O_{2-\delta}$ are presented in Fig. 1a and b, respectively in the form of pO_2–T–$\Delta\delta$ diagrams for the oxygen partial pressure range 10^{-4}–0.21 atm. with respect to a reference point of air. Under these more oxidizing conditions an increase in oxygen nonstoichiometry is observed with decreasing oxygen partial pressure and the magnitude of this increase exhibits negative temperature dependence. Larger increases in oxygen nonstoichiometry with decreasing pO_2 are observed at each temperature for the, Zr-free, $Ce_{0.8}Pr_{0.2}O_{2-\delta}$ composition than for the composition $Zr_{0.1}Ce_{0.7}Pr_{0.2}O_{2-\delta}$. This result compares well with previous results which showed depleted levels of atmospheric oxygen exchange for Zr-containing compositions assessed by thermogravimetric measurements in air [11].

Data categorising the nonstoichiometry of similar ceria-based defect fluorite materials, for example, pure $CeO_{2-\delta}$ or doped cerias such as Sm-, Gd-, or Y-ceria are well documented in the literature. For instance, gravimetric studies by authors such as Wang et al. [19] or Bevan et al. [20] demonstrate clearly that for either pure ceria or Gd doped-ceria materials, significant reduction of Ce^{4+} initiates at oxygen partial pressures lower than 10^{-10} atm, whereas at higher pO_2 values oxygen nonstoichiometry is observed to be effectively constant. In comparison, the materials of the present study contain two cations, Pr and Ce, which have capacity to exhibit mixed valency. In Fig. 1a and b oxygen nonstoichiometry can be seen to increase immediately as pO_2 decreases from air. It is therefore reasonable to suggest that the changes in oxygen nonstoichiometry observed at the much more oxidising conditions ($< 10^{-5}$ atm) in the current experiment are more likely related to the reduction of Pr^{4+} rather than severe destabilisation of Ce^{4+}. The dominant defect equilibrium at higher oxygen partial pressures is thereby suggested to be that of Pr reduction which is given by the equation

$$2Pr_{Ce}^{x} + O_{O}^{x} \overset{K}{\leftrightarrow} 2Pr'_{Ce} + V_{O}^{\bullet\bullet} + 1/2O_2, \quad (1)$$

where the Kröger Vink notation is used leading to the relationship describing equilibrium constant for Pr reduction

$$K = \frac{[V_{O}^{\bullet\bullet}][Pr'_{Ce}]^2 pO_2^{1/2}}{[Pr_{Ce}^{x}]^2[O_{O}^{x}]}. \quad (2)$$

Following the typical Brouwer approach [21] the electroneutrality relation under these higher oxygen partial

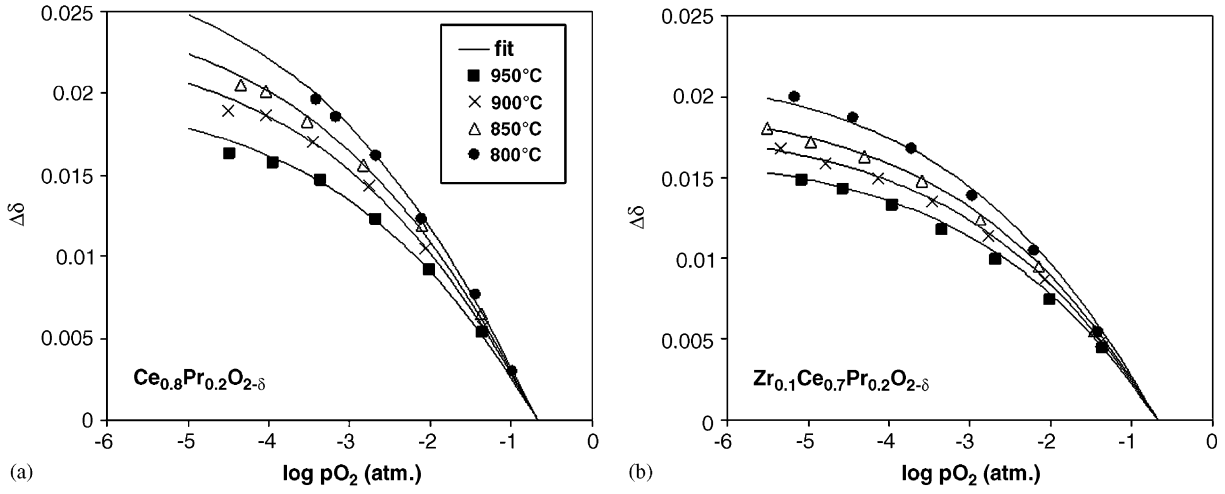

Fig. 1. The oxygen partial pressure dependence of oxygen nonstoichiometry with respect to a reference point of air, for the compositions (a) $Ce_{0.8}Pr_{0.2}O_{2-\delta}$ and (b) $Zr_{0.1}Ce_{0.6}Pr_{0.2}O_{2-\delta}$ from coulometric titration. Solid lines represent fit of data constrained by Eq. (7).

pressures can be simplified as

$$[Pr'_{Ce}] = 2[V^{\bullet\bullet}_{O}] \quad (3)$$

as $[Pr'_{Ce}] \gg [Ce'_{Ce}]$at high pO_2.

For any composition given by the general formula $Ce_{1-x}Pr_xO_{2-\delta}$ one can write the following relationships:

$$[O^x_O] = 2 - \delta, \quad (4)$$

$$[V^{\bullet\bullet}_{O}] = \delta \quad (5)$$

and using the electroneutrality relation Eq. (3)

$$[Pr^x_{Ce}] = x - 2\delta. \quad (6)$$

Clearly one can rewrite Eq. (2) to describe the pO_2 dependence of the oxygen nonstoichiometry, δ, using Eqs. (3)–(6), taking into account the fractional concentration of Pr (x),

$$K = \frac{4\delta^3 pO_2^{1/2}}{(x-2\delta)^2(2-\delta)}. \quad (7)$$

Values of K can subsequently be determined which best describe the experimental dependence of sample oxygen nonstoichiometry on pO_2, as presented in Fig. 1a and b, constrained by relationship, Eq. (7). The best-fit values of K are summarised in Table 1 whilst the solid lines describe the fit to the experimental data in Fig. 1a and b described by the equilibrium relationship given in Eq. (7). The fractional concentration of Pr in the 3+ oxidation state can be calculated as

$$\frac{[Pr'_{Ce}]}{[Pr_{Ce}]_{Total}} = \frac{2\delta}{x}. \quad (8)$$

Fig. 2a and b represent the pO_2 dependence of the fractional concentration of Pr in the 3+ oxidation state calculated for the values of equilibrium constant K given in Table 1. In oxidising conditions the fractional concentration of Pr^{3+} is shown to be much larger in the, Zr-containing, composition $Zr_{0.1}Ce_{0.7}Pr_{0.2}O_{2-\delta}$ than for $Ce_{0.8}Pr_{0.2}O_{2-\delta}$. It can be suggested that this is a factor resulting from ionic size. The ionic radii of Zr is much smaller than the Ce host lattice while the ionic radii of Pr in the 3+ oxidation state is much larger. The presence of a larger concentration of Pr^{3+} in the Zr-containing composition compensates for the presence of the smaller Zr ion. Fig. 2a and b also suggest that all Pr is reduced by 10^{-8} atm for both compositions.

3.2. Ionic conductivity

The modified e.m.f. technique takes the electrode polarisation into account and, thus, enables precise separation of the partial ionic and electronic contribution to the total conductivity [14–16]. The oxygen ion transference numbers (t_0) obtained for the samples $Zr_{0.1}Ce_{0.7}Pr_{0.2}O_{2-\delta}$ and $Ce_{0.8}Pr_{0.2}O_{2-\delta}$ by the e.m.f. method, averaged across a $p(O_2)$ gradient of 101/21 kPa (oxygen/air) are presented in Fig. 3a. A lower ionic transference number is shown for the Zr-containing composition. Combining transference numbers with the total conductivity (σ_T) values obtained by impedance spectroscopy at corresponding temperatures and oxygen partial pressure gradients, allows ionic conductivities to be estimated as

$$\sigma_0 = t_0\sigma_T. \quad (9)$$

The activation energy (E_a) for the partial ionic conductivities, Table 1, was calculated by the standard Arrhenius equation

$$\sigma_0 = \frac{A_0}{T}\exp\left[-\frac{E_a}{RT}\right], \quad (10)$$

where A_0 is the pre-exponential factor. Fig. 3b shows the respective ionic conductivity values for $Zr_{0.1}Ce_{0.7}Pr_{0.2}O_{2-\delta}$ and $Ce_{0.8}Pr_{0.2}O_2$ in oxygen potential gradients 101/21 kPa and 21 kPa/20 Pa. Decreasing temperature results in a decrease of ionic contribution to the total conductivity, in agreement with previous work on the system $Ce_{1-x}Pr_xO_{2-\delta}$ [8] by oxygen permeability measurements. At any temperature the ionic conductivity of the Zr-containing

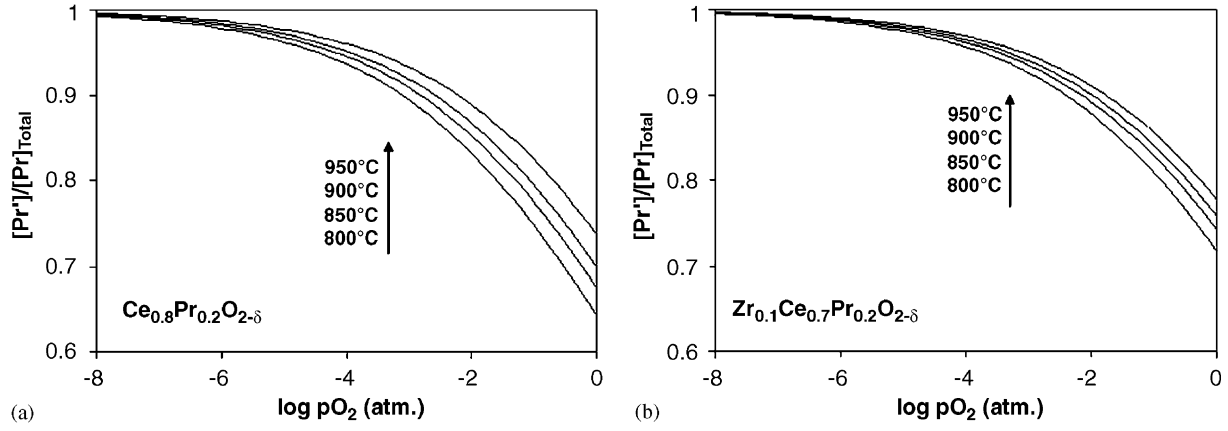

Fig. 2. Calculated oxygen partial pressure dependence of the fractional concentration of Pr in the 3+ oxidation state for (a) $Ce_{0.8}Pr_{0.2}O_{2-\delta}$ and (b) $Zr_{0.1}Ce_{0.6}Pr_{0.2}O_{2-\delta}$.

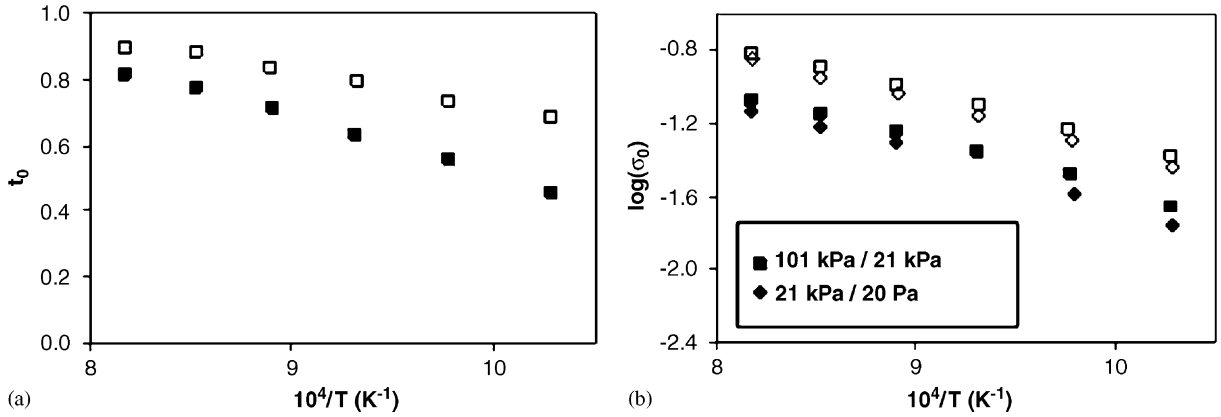

Fig. 3. The temperature dependence of (a) ion transference numbers under 101/21 kPa and (b) ionic conductivity under 101/21 kPa and 21 kPa/20 Pa oxygen partial pressure gradients for compositions $Ce_{0.8}Pr_{0.2}O_{2-\delta}$ (open symbols) and $Zr_{0.1}Ce_{0.6}Pr_{0.2}O_{2-\delta}$ (closed symbols).

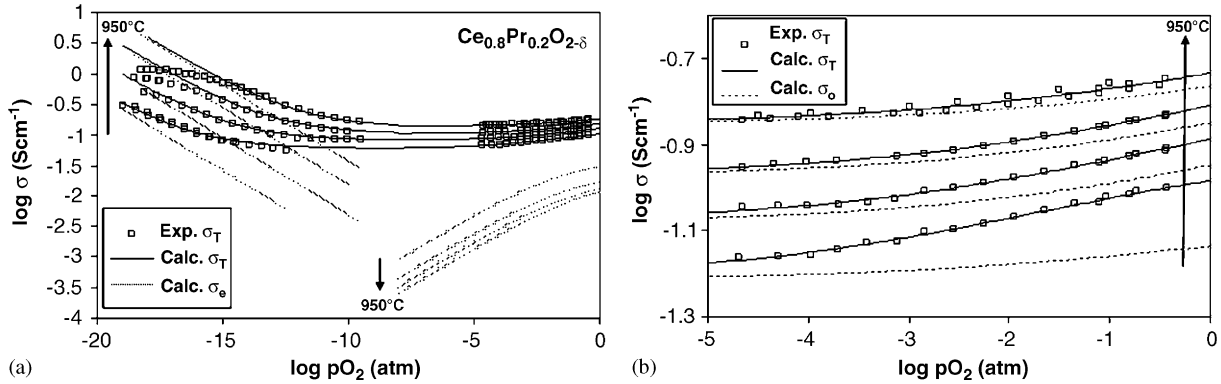

Fig. 4. Oxygen partial pressure dependence of total conductivity of $Ce_{0.8}Pr_{0.2}O_2$ at 950, 900, 850, 800 °C (arrows indicate direction of increasing temperature), dashed and solid lines indicate fit to experimental data (points). (a) Full pO_2 range, (b) in oxidising conditions.

composition is lower than it Zr-free counterpart. This is likely to be due to a combination of factors such as internal stresses due to the size mismatch of the small Zr ion with the host lattice and also that, from coulometric titration, we know that the Zr-containing composition contains a higher oxygen nonstoichiometry. A decrease in ionic conductivity with increasing vacancy concentration is typical of defect fluorite materials in the so called "concentrated regime" and is due to vacancy association [22]. Previously published results [11] by the e.m.f method for the sample $Zr_{0.1}Ce_{0.7}Pr_{0.2}O_{2-\delta}$, show that the ion transference number appears to be effectively unaffected by a change between the oxygen chemical potential gradients, 101/21 kPa (oxygen/air) to 21 kPa/20 Pa (air/argon) while a decrease in both electronic and ionic conductivities is shown. In Fig. 3b we extend these results to demonstrate that the composition $Ce_{0.8}Pr_{0.2}O_2$ exhibits a similar small decrease in ionic conductivity as pO_2 is reduced. The calculated activation energies for ionic conductivity shown in Table 1 are slightly larger in the more reducing partial pressure gradients for both compositions. This is typical for fluorite materials in the "concentrated regime" which show increases in activation energy with increasing vacancy concentration due to the presence of an enthalpy due to the dissociation of clustered vacancies in addition to the enthalpy of migration [22].

3.3. The pO_2 dependence of total conductivity

The pO_2 dependence of total conductivity is shown in Figs. 4a and b and 5a and b for the compositions $Ce_{0.8}Pr_{0.2}O_{2-\delta}$ and $Zr_{0.1}Ce_{0.6}Pr_{0.2}O_{2-\delta}$, respectively. For both compositions one observes a decrease in total conductivity with decreasing pO_2 at more oxidising values of pO_2, while the inverse trend is observable at low pO_2. Previous authors studying comparable Zr–Pr doped ceria materials [23,24] have suggested that these materials are predominantly electronic and that this total conductivity behaviour is due to a change between p-type electronic at high pO_2 to n-type electronic character at low pO_2. However, the oxygen ion transference numbers (t_0) obtained for the samples $Zr_{0.1}Ce_{0.7}Pr_{0.2}O_{2-\delta}$ and $Ce_{0.8}Pr_{0.2}O_{2-\delta}$ by the e.m.f. method in the previous section clearly show that these materials are predominantly ionic conductors at high pO_2. Furthermore, Fig. 3b shows that the ionic conductivity of these materials is lowered as pO_2

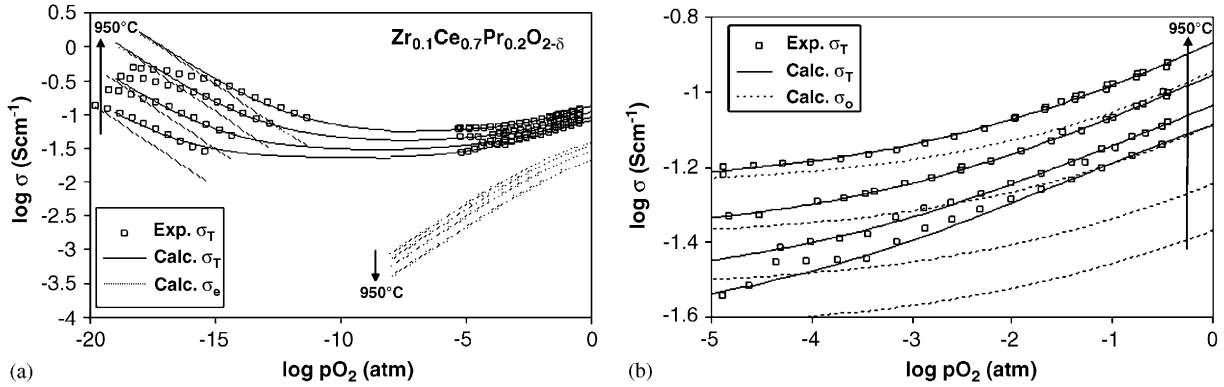

Fig. 5. Oxygen partial pressure dependence of total conductivity of $Zr_{0.1}Ce_{0.6}Pr_{0.2}O_{2-\delta}$ at, 950, 900, 850, 800 °C (arrows indicate direction of increasing temperature), dashed and solid lines indicate fit to experimental data (points). (a) Full pO_2 range, (b) in oxidising conditions.

Table 2
Fitting parameters for $Ce_{0.8}Pr_{0.2}O_{2-\delta}$ and $Zr_{0.1}Ce_{0.7}Pr_{0.2}O_{2-\delta}$ ceramics

T (°C)	$Ce_{0.8}Pr_{0.2}O_{2-\delta}$			$Zr_{0.1}Ce_{0.7}Pr_{0.2}O_{2-\delta}$		
	$K \pm 0.005$	$\kappa \pm 1$	$\ln \sigma_n^0 \pm 0.05\,S\,cm^{-1}$	$K \pm 0.005$	$\kappa \pm 1$	$\ln \sigma_n^0 \pm 0.05\,S\,cm^{-1}$
800	0.300	3.4	−3.9	0.500	14.0	−4.3
850	0.196	4.3	−4.3	0.390	12.7	−4.7
900	0.150	4.2	−4.8	0.320	10.8	−5.3
950	0.107	2.3	−5.3	0.240	9.2	−5.8

is decreased. One can categorically state therefore that the decrease in total conductivity with decreasing pO_2 in the high pO_2 range is predominantly due to a decreasing ionic conductivity. This result also emphasises the importance of using more than one technique to correctly analyse curves of pO_2 dependence of total conductivity.

3.3.1. Oxidising conditions

Following the discussion in Section 3.1, the electronic contribution in more oxidising conditions is given by the following relationship which describes the electronic conductivity to be proportional to the product of the concentration of charge carriers and the concentration of available sites to which small polaronic electron hops can progress between neighbouring Pr ions.

$$\sigma_e = K_e[Pr'_{Ce}](x - [Pr'_{Ce}]) \tag{11}$$

therefore, σ_e, the electronic contribution at any pO_2 can be expressed as

$$\sigma_e = [Pr'_{Ce}](x - [Pr'_{Ce}])\frac{\sigma_T^{air}(1 - t_0^{air})}{[Pr'_{Ce}]^{air}(x - [Pr'_{Ce}]^{air})}, \tag{12}$$

where σ_T^{air} is the total conductivity in air, and the unknown t_0^{air} is the transference number in air.

For the ionic conductivity under the same conditions we assume the following relationship, which describes a linear decrease in ionic conductivity with increasing vacancy concentration.

$$\frac{\partial \log \sigma_0}{\partial[V_O^{\bullet\bullet}]} = \kappa. \tag{13}$$

From comparison with literature data for doped cerias this assumption will be valid for small variations in vacancy concentration in the concentrated range, such as the level expected for the reduction of 20 at% Pr in the current materials under study [25,26]. The expression for the ionic conductivity σ_0 at any pO_2 can therefore be stated as

$$\log \sigma_0 = \log(\sigma_T^{air} t_0^{air}) - (\kappa(\delta^{air} - \delta)). \tag{14}$$

Least-squares fitting of Eqs. (12) and (14) allows the unknowns t_0^{air} and κ to be determined. Under these more oxidising conditions, fitted curves (solid lines) for σ_e, σ_0 and $\sigma_T = \sigma_0 + \sigma_e$ are shown to fit well the experimental data (points) in Figs. 4a and b for the composition $Ce_{0.8}Pr_{0.2}O_{2-\delta}$ and Figs. 5a and b for the composition $Zr_{0.1}Ce_{0.7}Pr_{0.2}O_{2-\delta}$, respectively. Corresponding fitted values of κ are given in Table 2.

Fig. 6 compares the vacancy concentration dependence of ionic conductivity at 900 °C for $Zr_{0.1}Ce_{0.7}Pr_{0.2}O_{2-\delta}$ and $Ce_{0.8}Pr_{0.2}O_{2-\delta}$ upon reduction, with literature data for Gd-doped CeO_2 and Sm-doped CeO_2 [25,26]. Values of κ for both compositions of this study and also that for Sm–CeO_2 for compositions deep within the concentrated vacancy range are presented on the chart. The calculated value of κ for the composition $Zr_{0.1}Ce_{0.7}Pr_{0.2}O_{2-\delta}$ is similar to the

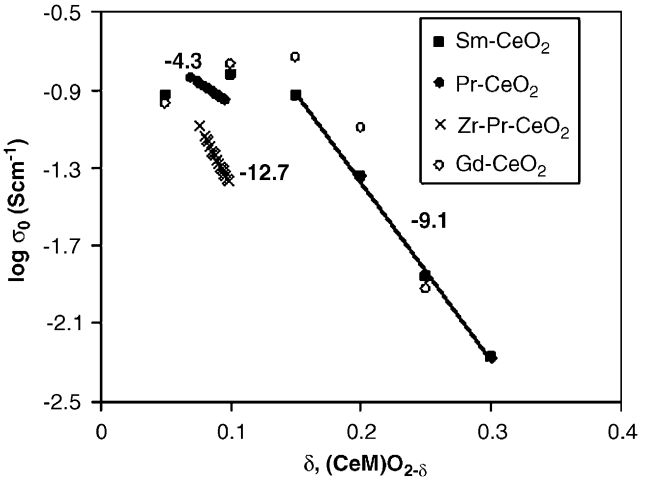

Fig. 6. Comparison of the vacancy concentration dependence of ionic conductivity at 900 °C for $Zr_{0.1}Ce_{0.7}Pr_{0.2}O_{2-\delta}$ and $Ce_{0.8}Pr_{0.2}O_{2-\delta}$ upon reduction, with literature data in air for Gd-doped CeO_2 and Sm-doped CeO_2 [25,26]. Calculated values of κ are presented.

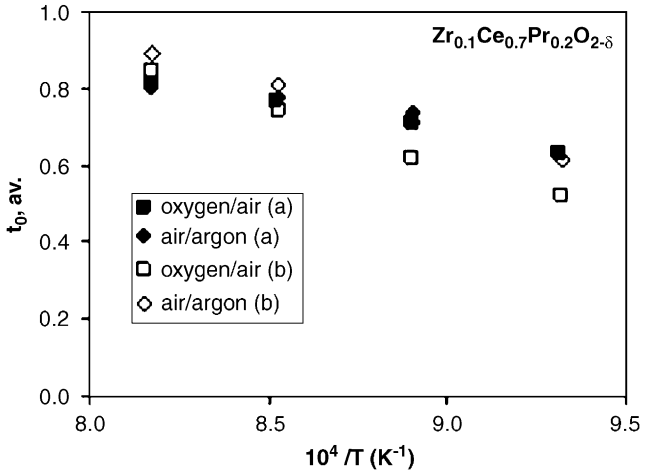

Fig. 7. Comparison of the average transference number (t_0, av) for the composition $Zr_{0.1}Ce_{0.7}Pr_{0.2}O_{2-\delta}$ under the oxygen partial pressure gradients 101/21 kPa (oxygen/air) and 21 kPa/20 Pa (air/argon) obtained by e.m.f. measurements (a) with those calculated using Eq. (15) from fitted results of conductivity vs. pO_2 measurements (b).

literature materials of high vacancy concentration, while the value of κ for the Zr-free composition $Ce_{0.8}Pr_{0.2}O_{2-\delta}$ is shown to be lower and comparable to the gradient of the literature curves close to the conductivity maxima for the concentrated range. A decrease in ionic conductivity in the concentrated range is characteristic of increasing pre-exponential factor and also increasing activation energy for conduction due to the association of vacancies [22]. The result that Zr-containing compositions exhibit a higher dependence of ionic conductivity on vacancy concentration (larger value of κ) corresponds well with higher activation energies for ionic conductivity reported in Table 1 for this composition from the modified e.m.f. technique. This suggests that vacancy association is favoured in the Zr-containing composition, and this is probably as a result of the large size mismatch of Zr with the host lattice.

For measurements under a nonzero oxygen pressure gradient, such as in the e.m.f. technique, the transference numbers are averaged in a given range of oxygen chemical potentials (μ): where the values of μ_1 and μ_2 correspond to $p(O_2)$ values at the electrodes. Therefore, to compare values of transference numbers obtained by the e.m.f. technique in Section 3.2 and those calculated in this section from fitting of conductivity vs. pO_2 measurements one must first calculate the transference number averaged across the same oxygen partial pressure gradients as experienced in the e.m.f. measurements by the following equation:

$$t_{0,\mathrm{av}} = \frac{1}{\mu_2 - \mu_1}\int_{\mu_1}^{\mu_2} \frac{\sigma_0}{\sigma_T}\,\mathrm{d}\mu, \tag{15}$$

where σ_0 and $\sigma_T = \sigma_0 + \sigma_e$ are values calculated from Eqs. (11)–(14). As an example the average transference number (t_0, av) for the composition $Zr_{0.1}Ce_{0.7}Pr_{0.2}O_{2-\delta}$ under the oxygen partial pressure gradients 101/21 kPa (oxygen/air) and 21 kPa/20 Pa (air/argon) from e.m.f. measurements are compared in Fig. 7 to those calculated using Eq. (15) from fitted results of conductivity vs. pO_2 measurements. A reasonable correlation of average transference number between the two techniques is shown; especially when one considers that the fitted results for the conductivity vs. pO_2 measurements have their base in results derived from a further experiment which determined the pO_2 dependence of nonstoichiometry by coulombic titration.

3.3.2. Reducing conditions

Fig. 2a and b, conclude from our model that all praseodymium will be reduced under values of pO_2 lower than 10^{-8} atm, hence preventing electronic conductivity from small polaronic hopping between neighbouring Pr ions, as expressed by Eq. (11). The enhancement of total conductivity observed in Figs. 4a and 5a, in more reducing conditions must therefore be a factor of the reduction of Ce^{4+}, in agreement with literature data on similar ceria based defect fluorite materials [19,20] which show reduction of Ce^{4+} initiating at pO_2 values lower than 10^{-10} atm, as stated in Section 3.1. A similar defect model can therefore be suggested as in Refs. [19,20] for the reduction reaction of ceria solid solutions which contain a trivalent dopant, in our case this trivalent dopant is now Pr^{3+} under these reducing conditions. The reduction reaction of Ce^{4+} can therefore be expressed as

$$2Ce_{Ce}^{x} + O_O^{x} \overset{K_2}{\leftrightarrow} 2Ce'_{Ce} + V_O^{\bullet\bullet} + 1/2\,O_2. \tag{16}$$

Applying the law of mass action leads to the relationship describing the equilibrium constant for Ce reduction

$$K_2 = \frac{[V_O^{\bullet\bullet}][Ce'_{Ce}]^2 pO_2^{1/2}}{[Ce_{Ce}^{x}]^2[O_O^{x}]} \tag{17}$$

The electroneutrality equation in this case

$$[Ce'_{Ce}] + [Pr'_{Ce}] = 2[V^{\bullet\bullet}_{O}] \quad (18)$$

can be simplified for low reductions of Ce by the assumptions that the vacancy concentration is dominated by the concentration of Pr^{3+}

$$2[V^{\bullet\bullet}_{O}] \approx [Pr'_{Ce}] \approx \text{constant} \quad (19)$$

and that the concentration of $[Ce^{x}_{Ce}]$ and $[O^{x}_{O}]$ can be omitted from Eq. (17) because they are large enough to be considered constant for such low levels of Ce reduction. The combination of these assumptions leads to the prediction that at low reductions of Ce the concentration of n-type charge carriers will have a pO_2 dependence of $-1/4$ such as

$$[Ce'_{Ce}] \propto pO_2^{-1/4}. \quad (20)$$

The total conductivity in reducing conditions can therefore be expressed as

$$\sigma_T = \sigma^0_n pO_2^{-1/4} + \sigma_0, \quad (21)$$

where the n-type conductivity (σ_n) is described by the product $\sigma^0_n pO_2^{-1/4}$ (where σ^0_n is a constant), and σ_0 represents the ionic conductivity. The p-type conductivity is assumed negligible in these reducing conditions. The ionic conductivity for low reductions of Ce is taken to be constant and to have the value of the ionic conductivity when all Pr is in the 3+ oxidation state at 10^{-8} atm. The fitted curves for the n-type conductivity and the total conductivity in reducing conditions are shown in Figs. 4a and 5a as the dashed and solid lines, respectively. At the highest temperatures deviation between the fit and the experimental results can be observed as the assumptions used in the simplification of the electroneutrality equation Eq. (19) are exceeded. A similar trend is observed in literature data of similar ceria-based defect fluorite materials [27]. It should be noticed that incorporation of the nonsimplified electroneutrality equation, Eq. (18), in the mass action relation, Eq. (17), will serve to lower the power law dependence of the n-type conductivity. Furthermore, defect interactions such as vacancy ordering and defect association, can also be considered to occur in the Ce(ZrPr)O_2 materials as significant concentrations of Ce become reduced.

3.4. The pO_2 dependence of thermoelectric power

The total thermoelectric power, Q_t, for a mixed conductor is normally expressed as [28]

$$Q_t = t_0 Q_0 + \sum_j t_j Q_j, \quad (22)$$

where t_j and Q_j (j = p, n) are the transference numbers and the partial thermoelectric power of an electronic carrier j, while t_0 and Q_0 express these terms for the ionic species.

Discussion in the previous sections described how the dominant charge carriers in reducing and in oxidising conditions can be considered to be distinct. For this reason, discussion of the pO_2 dependence of the thermoelectric power is similarly split into two distinct pO_2 regimes.

At higher oxygen partial pressures the dominant charge carrier is that of praseodymium, which undergoes reduction on decreasing pO_2 as described by Eq. (1). In this region the total thermoelectric power can be simplified [29] as

$$Q_t = t_p \frac{R}{F} \ln\left(\frac{N}{p}\right) + t_0\left(-\frac{R}{4F}\ln(pO_2) + Q^0_{O^{2-}}\right) \quad (23)$$

assuming a hopping conduction for electrons [30], where N is the density of states, t_p and t_0 are the p-type electronic and ionic transference numbers, respectively, and $Q^0_{O^{2-}}$ is the ionic thermopower at unit pO_2. The experimental data of total thermoelectric power were fitted as a function of pO_2 by combination of the pO_2 dependence of the concentration of charge carriers, p, obtained from coulometric titration, Eqs. (6) and (7), and the transference numbers calculated on fitting the total conductivity data using Eqs. (11)–(14), such that the transference numbers are given by $t_0 = \sigma_0/\sigma_p + \sigma_0$ and $t_p = \sigma_p/\sigma_p + \sigma_0$. Regression parameters were N and $Q^0_{O^{2-}}$.

At lower oxygen partial pressures the dominant charge carrier is that of Ce^{3+}, following the reduction reaction expressed by Eq. (14). The total thermoelectric power in this region can be stated as

$$Q_t = t_n\left(-\frac{R}{4F}\ln(pO_2) + Q^0_n\right) + t_0\left(-\frac{R}{4F}\ln(pO_2) + Q^0_{O^{2-}}\right), \quad (24)$$

where the transference numbers are given by $t_0 = \sigma_0/\sigma_n + \sigma_0$ and $t_n = \sigma_n/\sigma_n + \sigma_0$ from Eq. (20). Regression parameters were $Q^0_{O^{2-}}$ and Q^0_n, values of σ^0_n were fixed to the values calculated by fitting total conductivity data using, Eq. (21).

In this way good fits of the total thermoelectric power can be obtained in both reducing and oxidising conditions, as shown in Fig. 8a and b, and have their basis in the defect relations proposed to explain the pO_2 dependence of total conductivity Eqs. (1)–(8), (11)–(14) and (16)–(21). In the most heavily reducing conditions and at the highest temperatures deviation of the fit from the experimental data can be observed as the assumptions used in the simplification of the electroneutrality equation Eq. (19) are exceeded, as was also observed in the fit of the total conductivity measurements and can be explained by the same reasoning.

4. Conclusions

The influence of substitution of 10 at% Zr for cerium in $Ce_{0.8}Pr_{0.2}O_{2-\delta}$ to form $Zr_{0.1}Ce_{0.7}Pr_{0.2}O_{2-\delta}$ upon resultant mixed conductivity has been analysed. The fractional concentration of Pr in the 3+ oxidation state has been calculated from results of coulometric titration to be much larger for the Zr-containing composition. Reducing pO_2

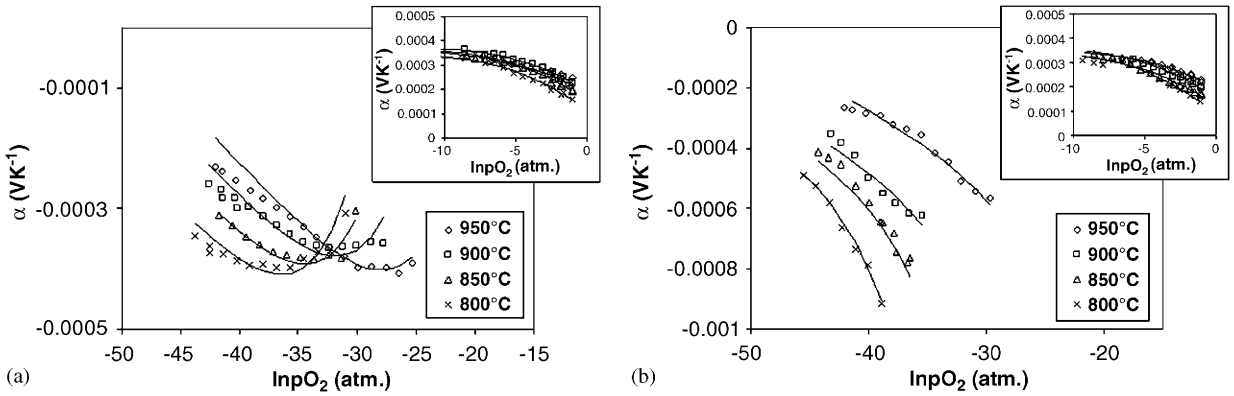

Fig. 8. Oxygen partial pressure dependence of total thermoelectric power of (a) $Ce_{0.8}Pr_{0.2}O_{2-\delta}$ and (b) $Zr_{0.1}Ce_{0.6}Pr_{0.2}O_{2-\delta}$. Solid lines represent fit to experimental data (points).

leads to further increases in oxygen nonstoichiometry and the magnitude of this increase shows negative temperature dependence. At any temperature composition $Ce_{0.8}Pr_{0.2}O_{2-\delta}$ shows larger increases in nonstoichiometry with decreasing pO_2 than its Zr-containing counterpart. In oxidising conditions, measurements of oxygen concentration cell e.m.f. combined with impedance spectroscopy reveal a decrease in both ionic and electronic conductivities with decreasing pO_2 and a positive temperature dependence of measured ion transference numbers, t_0. In oxidising conditions these materials are predominantly ionic conductors, with lower values of t_0 and depleted ionic, electronic and total conductivities exhibited by the Zr-containing composition. In more oxidising conditions, depletion of total conductivity with decreasing pO_2 results from a decreasing ionic conductivity due to the reduction of praseodymium and creation of oxygen ion vacancies, whereas enhancement of the total conductivity in more reducing conditions is related to increased n-type conductivity upon the reduction of cerium.

Acknowledgments

This work was supported by the FCT, Portugal (Projects POCTI/CTM/39381/2001 and SFRH/BPD/3529/2000) and the NATO Science for Peace program (Project 978002).

References

[1] A.D. Logan, M. Shelef, J. Mater. Res. 9 (1994) 468.
[2] M.Y. Sinev, G.W. Graham, L.P. Haack, M. Shelef, J. Mater. Res. 11 (1996) 1960.
[3] P. Knauth, H.L. Tuller, J. Eur. Ceram. Soc. 19 (1999) 831.
[4] M. Rajendran, K.K. Mallick, A.K. Bhattacharya, J. Mater. Sci. 33 (1998) 5001.
[5] T.S. Stefanik, H.L. Tuller, J. Eur. Ceram. Soc. 21 (2001) 1967.
[6] C.K. Narula, L.P. Haack, W. Chun, H.W. Jen, G.W. Graham, J. Phys. Chem. B 103 (1999) 3634.
[7] S. Rossignol, C. Descorme, C. Kappenstein, D. Duprez, J. Mater. Chem. 11 (2001) 2587.
[8] P. Shuk, M. Greenblatt, Solid State Ionics 116 (1999) 217.
[9] M. Nauer, C. Ftikos, B.C.H. Steele, J. Eur. Ceram. Soc. 14 (1994) 493.
[10] C. Ftikos, M. Nauer, B.C.H. Steele, J. Eur. Ceram. Soc. 12 (1993) 267.
[11] D. Fagg, V.V. Kharton, A. Shaula, I.P. Marozau, J.R. Frade, Solid State Ionics 176 (2005) 1723.
[12] M.V. Patrakeev, E.B. Mitberg, A.A. Lakhtin, I.A. Leonidov, V.L. Kozhevnikov, V.V. Kharton, M. Avdeev, F.M.B. Marques, J. Solid State Chem. 167 (2002) 203.
[13] F.M.B. Marques, G.P. Wirtz, J. Am. Ceram. Soc. 75 (1992) 369.
[14] V.P. Gorelov, Elektrokhimiya 24 (1988) 1380 (in Russian).
[15] V.V. Kharton, F.M.B. Marques, Solid State Ionics 140 (2001) 381.
[16] V.V. Kharton, A.P. Viskup, F.M. Figueiredo, E.N. Naumovich, A.A. Yaremchenko, F.M.B. Marques, Electrochim. Acta 46 (2001) 2879.
[17] V.V. Kharton, E.N. Naumovich, A.A. Vecher, A.V. Nikolaev, J. Solid State Chem. 120 (1995) 128.
[18] M.H.R. Lankhorst, H.J.M. Bouwmeester, J. Electrochem. Soc. 144 (4) (1997) 1268.
[19] S. Wang, H. Inaba, H. Tagawa, M. Dokiya, T. Hashimoto, Solid State Ionics 107 (1998) 73.
[20] D.J.M. Bevan, J. Kordis, J. Inorg. Nucl. Chem. 26 (1964) 1509.
[21] G. Brouwer, Philips Res. Rep. 9 (1954) 366.
[22] J.A. Kilner, B.C.H. Steele, in: O. Toft Sørensen (Ed.), Non-Stoichiometric Oxides, Academic Press, New York, 1981, p. 233.
[23] X.Q.Y.S. Lin, C.T. Holt, S.L. Swartz, J. Mater. Sci. 38 (2003) 1073.
[24] T.S. Stefanik, H.L. Tuller, J. Electroceram. 13 (2004) 799.
[25] T. Kudo, H. Obayashi, J. Electrochem. Soc. 123 (3) (1976) 415.
[26] H. Yahiro, Y. Eguchi, K. Eguchi, H. Arai, J. Appl. Electrochem. 18 (1988) 527.
[27] D. Schneider, M. Gödickemeier, L.J. Gauckler, J. Electroceram. 1 (2) (1997) 165.
[28] H.-I. Yoo, J.-H. Hwang, J. Phys. Chem. Solids 52 (1992) 973.
[29] G.H. Jonker, Philips Res. Rep. 23 (1968) 131.
[30] D.R. Goldschmidt, H. Tuller, Cryst. Latt. Def. Amorph. Mater. 15 (1987) 203.